

Novel ultra-stable and highly luminescent white light-emitting diodes from perovskite quantum dots—Polymer nanofibers through biaxial electrospinning

Cite as: APL Mater. 7, 111105 (2019); <https://doi.org/10.1063/1.5124880>

Submitted: 17 August 2019 . Accepted: 25 October 2019 . Published Online: 13 November 2019

Dai-Hua Jiang, Yi-Hsuan Tsai, Loganathan Veeramuthu , Fang-Cheng Liang, Lung-Chin Chen, Chun Che Lin, Toshifumi Satoh , Shih-Huang Tung, and Chi-Ching Kuo 

COLLECTIONS

Paper published as part of the special topic on [Light Emission from Perovskite Materials](#)

Note: This paper is part of the Special Issue on Light Emission from Perovskite Materials.



View Online



Export Citation



CrossMark

ARTICLES YOU MAY BE INTERESTED IN

[One-step solution synthesis of white-light-emitting films via dimensionality control of the Cs-Cu-I system](#)

APL Materials **7**, 111113 (2019); <https://doi.org/10.1063/1.5127300>

[Performance boosting strategy for perovskite light-emitting diodes](#)

Applied Physics Reviews **6**, 031402 (2019); <https://doi.org/10.1063/1.5098871>

[Hole selective materials and device structures of heterojunction solar cells: Recent assessment and future trends](#)

APL Materials **7**, 110701 (2019); <https://doi.org/10.1063/1.5121327>

APL Materials *Excellence in Research Award*

[LEARN MORE >>](#)

Novel ultra-stable and highly luminescent white light-emitting diodes from perovskite quantum dots—Polymer nanofibers through biaxial electrospinning

Cite as: APL Mater. 7, 111105 (2019); doi: 10.1063/1.5124880

Submitted: 17 August 2019 • Accepted: 25 October 2019 •

Published Online: 13 November 2019



View Online



Export Citation



CrossMark

Dai-Hua Jiang,^{1,2,3,a)} Yi-Hsuan Tsai,^{1,a)} Loganathan Veeramuthu,¹  Fang-Cheng Liang,¹ Lung-Chin Chen,¹ Chun Che Lin,^{1,4} Toshifumi Satoh,^{3,b)}  Shih-Huang Tung,^{2,b)} and Chi-Ching Kuo^{1,b)} 

AFFILIATIONS

¹Institute of Organic and Polymeric Materials, Research and Development Center of Smart Textile Technology, National Taipei University of Technology, 10608 Taipei, Taiwan

²Institute of Polymer Science and Engineering, National Taiwan University, 10617 Taipei, Taiwan

³Faculty of Engineering, Hokkaido University, Sapporo 060-8628, Japan

⁴Graduate Institute of Nanomedicine and Medical Engineering and International Ph.D. Program in Biomedical Engineering, College of Biomedical Engineering, Taipei Medical University, Taipei 110, Taiwan

Note: This paper is part of the Special Issue on Light Emission from Perovskite Materials.

a) Contributions: D.-H. Jiang and Y.-H. Tsai contributed equally to this work.

b) Authors to whom correspondence should be addressed: satoh@eng.hokudai.ac.jp; shtung@ntu.edu.tw; and kuocc@mail.ntut.edu.tw. Tel.: 886-2-27712171*2407. Fax: 886-2-27317174.

ABSTRACT

Cesium lead halide perovskite quantum dots (QDs) have drawn extensive attention due to their excellent optical properties. However, their use is limited by poor stability. To enhance their stability, we electrospun perovskite-embedded fibers from composite CsPbX₃ (X = Cl, Br, and I) perovskite QDs, blending with three polymers, poly(styrene-butadiene-styrene) (SBS), poly(methyl methacrylate) (PMMA), or polystyrene (PS), for the light-emitting diode (LED) applications. We found that the stretchable CsPbBr₃@SBS fibers revealed the highest photoluminescence quantum yield, the CsPbBr₃@PMMA fibers demonstrated a high thermal stability, and the CsPbBr₃@PS fibers exhibited the best water-resistant stability. The photoluminescence intensity maintained 83% of its initial intensity for more than 3 months in water. Furthermore, the LED devices are manufactured from the blue chips and packaged with the core/shell red and green perovskite-based fibers by using biaxial electrospinning exhibited stable and highly efficient white luminescence. The luminance and efficiency are higher than 400% of the values of multilayered structures.

© 2019 Author(s). All article content, except where otherwise noted, is licensed under a Creative Commons Attribution (CC BY) license (<http://creativecommons.org/licenses/by/4.0/>). <https://doi.org/10.1063/1.5124880>

I. INTRODUCTION

The efficient photovoltaic cells based on organometal halide perovskites were demonstrated for the first time in 2009.¹ Since then, the organic/inorganic hybrid lead halide perovskites have attracted extensive attention worldwide for optoelectronic device applications. Organic/inorganic perovskite materials possess

excellent optoelectronic and photovoltaic properties, such as a high photoluminescence quantum yield (PLQY), long lifetime, narrow emission bandwidth, and tunable light emission. Such advantages can be applied to light-emitting diode (LED) devices, transistor devices, solar cells, nanolasers, and bioimaging.^{2–7} However, perovskites suffer from poor stability due to their ionic nature that is sensitive to moisture and low melting temperature, which

has raised major concerns about their large-scale applicability.^{8,9} Therefore, the practical use of perovskites usually requires additional protective strategies to overcome degradation in the ambient atmosphere.

Numerous methods have been applied to enhance the stability of perovskites, such as the macroscale polymer matrix method,¹⁰ protective coatings,^{4,11,12} synthetic modification,¹³ and polymer blends.^{14–16} However, to date, only limited progress has been made in enhancing the stability. In practice, dense polymer matrices endow water-sensitive materials with hydrophobic characteristics. Encapsulation by a polymer matrix is an effective strategy to improve the stability of perovskite quantum dots (QDs), especially water resistance. For example, Wu *et al.*¹⁵ reported that a swelling-deswelling microencapsulation strategy could thoroughly disperse organic–inorganic perovskite nanoparticles. The PLQY could be as high as 48%, and the device could be immersed in boiling water and still maintain more than 65% of its initial brightness after 5 h. Chen *et al.*¹⁷ reported that the composite nano-/micrometer beads of perovskite quantum dots embedded in polystyrene showed similar phenomena and could be combined with cross-linked PS beads to retain 68% of the PLQY. The composites remained strongly luminescent after being immersed in water for over 9 months. Furthermore, even when immersed in acid/alkali aqueous solution, phosphate buffer solution, and Dulbecco's modified eagle medium biological buffer, this type of device still emitted high luminescence. Alivisatos *et al.*¹³ revealed a ligand-assisted modification technique to produce perovskite QDs by grafting long alkyl ligand chains onto surfaces that interacted with hydrophobic polymers to enhance water stability. Moreover, the conditions of polarization and color

tunable properties could be achieved by changing the morphology of the nanocrystalline component. Zhang *et al.*¹⁰ used a one-pot strategy to make perovskite-polymer composites that were stable and maintained a PLQY higher than 60%. A white device was also successfully prepared by the perovskite–polymer composites. Despite these advances, the search of other facile methods is ongoing in the hope of achieving a commercially viable preparation for perovskite materials that would be suitable for optoelectronic devices.

Different from typical thin-film preparation methods, electrospinning (ES) is a technique that has been widely used to prepare fibers because of its low-cost, simple operation, and capability of fine-tuning the morphology of the fibers in nano- to microscale. Because ES can produce fibers with high surface-to-volume ratios, the ES fibers are good candidates for sensory applications. For the past several years, diverse fluorescent sensory applications based on conjugated polymer nanofibers have been successfully prepared by our group.^{18–21} Another important effect of ES fibers is the geometrical confinement to the implants embedded in the fibers, which can adjust the orientation, crystallinity, stability, and optoelectronic properties of the implants. Furthermore, the diameter and morphology of the fibers can be easily controlled by ES parameters.^{18–20} Functional materials such as metallic nanoparticles,^{18,21,22} conjugated polymers,^{23–25} perovskite,¹⁹ and QDs²⁶ can be incorporated into ES fibers to prepare composite fibers for various device applications. For example, Chen *et al.*¹⁹ exploited the one-step coaxial ES technique to fabricate the perovskite and polymer in the core/shell nanofibers. Owing to the hydrophobic characteristics of the shell polymer, the perovskite crystals in the core are

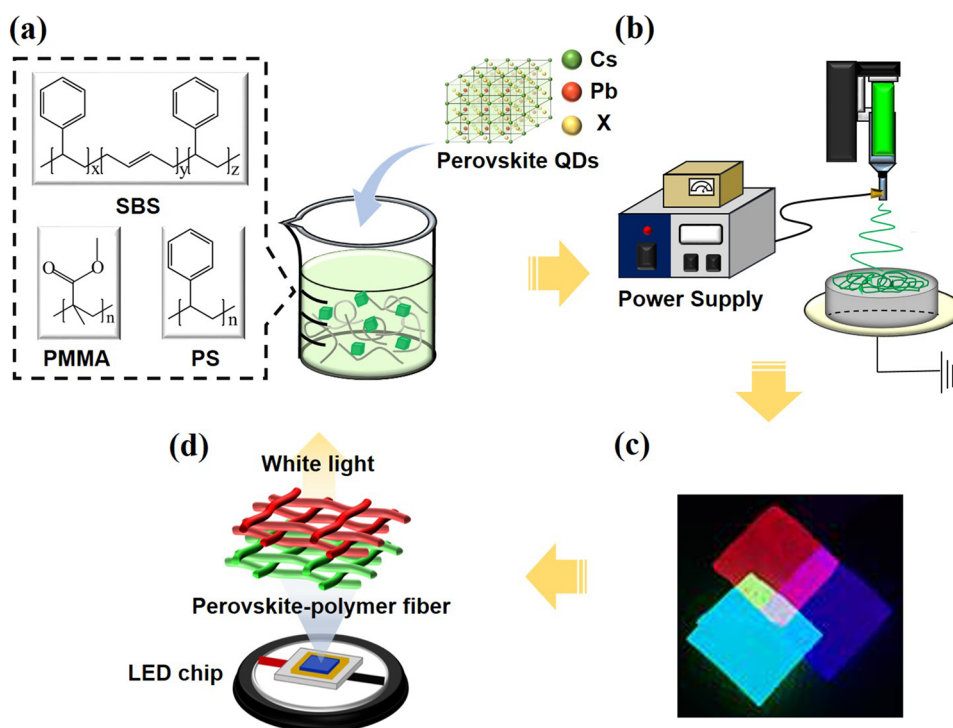


FIG. 1. [(a) and (b)] Schematic of the CsPbX₃ (X = Cl, Br, I) nanofiber fabrication process. (c) Optical image of blue, green, and red composite nanofibers under UV-light (365 nm) excitation. (d) Schematic for the configuration of the prototype WLED device.

highly stable in the atmosphere and the aggregation is mitigated due to geometrical confinement. The PLQY of perovskite nanofiber is 30.9%, and the photoluminescence intensity can retain 50% of the initial intensity when it is immersed in water for 48 h. Furthermore, our group²⁶ successfully used the fibrous mats packaging approach in bright perovskite LEDs. The correlated color temperatures (CCT) of white LEDs (WLEDs) can be easily controlled by adjusting the thickness of the nanofibers and the voltage. Given these advantages, we proposed that ES is a suitable method to stably maintain the pristine optical properties of perovskites. We thus investigated the effects of polymers on perovskites embedded in fibers, which is a topic that has not been thoroughly explored.

In this study, we exploited a simple strategy to prepare perovskite-polymer fibers, that is, the electrospinning of the composite fibers from the solutions where the perovskite QDs and

polymer are mixed. We used three polymers, including poly(styrene-butadiene-styrene) (SBS), which is a rubber and can be easily prepared into ES fibers, poly(methyl methacrylate) (PMMA), which is a highly transparent polymer with high glass transition temperature, and polystyrene (PS), which is highly stable when immersed in water due to its hydrophobic characteristics. We further used the biaxial electrospinning method to create the core/shell structure in the fibers, where red perovskite materials serve as the core and green materials serve as the shell. The fibrous mats were used to package the blue LED chips to obtain efficient perovskite-based WLEDs. Unexpectedly, the luminance and efficiency of the core/shell WLED devices are as high as 430% and 420% of the values of the multilayered devices, respectively. The approach reported herein provides a promising avenue to fabricate stable and highly efficient perovskite-based WLEDs.

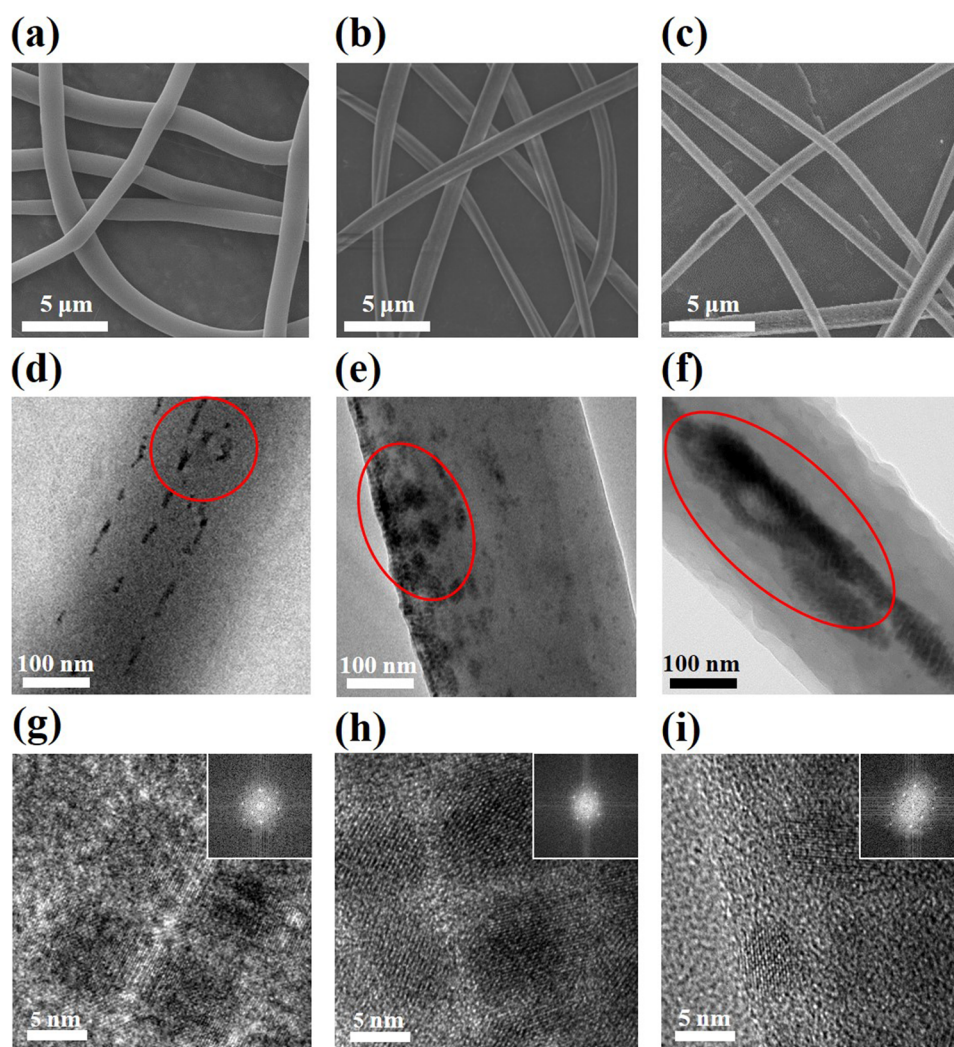


FIG. 2. The SEM images of (a) CsPbBr₃@SBS fiber, (b) CsPbBr₃@PMMA fiber, and (c) CsPbBr₃@PS fiber. The TEM images of (d) CsPbBr₃@SBS, (e) CsPbBr₃@PMMA, and (f) CsPbBr₃@PS. The HRTEM images and a fast Fourier-transform image of (g) CsPbBr₃@SBS, (h) CsPbBr₃@PMMA, and (i) CsPbBr₃@PS.

II. RESULTS AND DISCUSSION

The solutions for electrospinning were prepared from a stock solution of colloidal CsPbX₃ perovskite QDs in toluene (200 μ l, \sim 20 mg ml⁻¹) mixed with polymers (SBS, PMMA, or PS) in dichloromethane (DCM) (1 ml, \sim 15 wt. %), as illustrated in Fig. 1(a). The QDs can be well dispersed, and polymers can be dissolved in the mixed solutions without precipitation. Figure 1(b) shows the schematic of the uniaxial ES setup with the mixed solutions. The feed rate and voltage for the ES process were 0.8–1.0 ml h⁻¹ and 12.4 kV, respectively. The colors of the perovskite–polymer fibers were tuned by adjusting halide ratios. The red, green, and blue fibrous mats are displayed in Fig. 1(c), which, as the primary colors, can mix to produce other colors. Subsequently, the perovskite–polymer fibrous mats were applied in blue LED chips to radiate while light, as shown in Fig. 1(d).

A. Characterization of perovskite fibers

The SEM images of the fibers with CsPbBr₃ perovskite QDs embedded are shown in Figs. 2(a)–2(c). The average diameters of the fibers were approximately 1 μ m. The elemental analyses of the perovskite–polymer fibers are provided in Fig. S1. The data confirmed that the perovskites were successfully encapsulated in the fibers, as evidenced by the signals of Cs, Pb, and halogens. The TEM images that reveal the distribution of the perovskite QDs in the fibers are shown in Figs. 2(d)–2(f). The perovskite crystals can be clearly distinguished from the polymer matrices owing to the higher electron density. Among the fibers, CsPbBr₃@SBS exhibited less aggregation of the QDs, and we speculated that the better dispersion is because SBS contains polybutadiene hydrocarbon segments that are more compatible with the ligands (oleylamine and oleic acid) on the QD surface, similar to the phenomena reported previously.¹³ The severest aggregation occurred in CsPbBr₃@PS fibers, indicating the low compatibility between the ligands and PS.

High-resolution TEM (HRTEM) was used to investigate the perovskite crystals, as shown in Figs. 2(g)–2(i) and S2. The insets in Figs. 2(g)–2(i) are the fast Fourier transformation patterns from the HRTEM images. The CsPbBr₃ crystals were cubic phase with an average size of 9 ± 1 nm and a d-spacing of 0.58 nm for the (100) plane. After electrospinning, the particle size was similar to the size of the original perovskite QDs.^{27,28} Figure 3 shows the XRD profiles of CsPbBr₃ QD-based fibers and CsPbBr₃ QDs. The diffraction peaks of the CsPbBr₃ QDs in all the polymers appear exactly at the same 2θ with those of CsPbBr₃ QDs,²⁹ indicating that the structures of the perovskite QDs were unchanged after

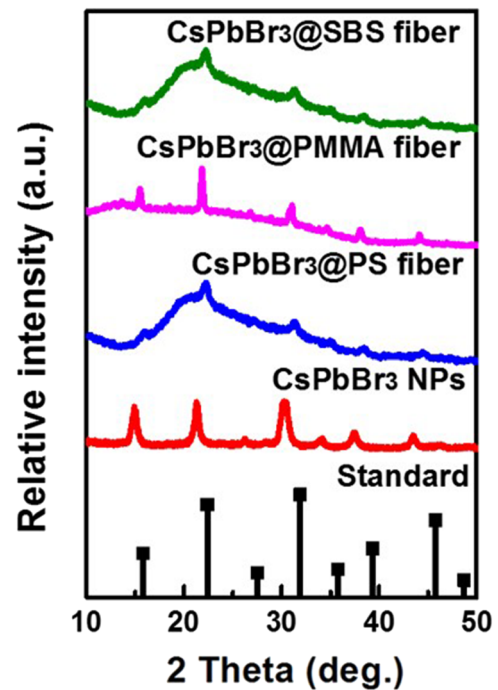


FIG. 3. The XRD patterns of CsPbBr₃@SBS, CsPbBr₃@PMMA, CsPbBr₃@PS, and CsPbBr₃ NPs standard JCPDS.

electrospinning. The broad humps below $2\theta = 40^\circ$ found in the profiles of the fibers are the scattering halos produced by the amorphous polymers. We further conducted optical imaging for green CsPbBr₃ and red CsPb(Br_{0.4}I_{0.6})₃ perovskite–polymer fibers, which were excited by ultraviolet light at 405 nm wavelength. As presented in Fig. S3, the perovskites in all the fibers emitted their original light colors, which verified that they retained the fluorescent properties after electrospinning.

The contact angles of neat polymer and CsPbBr₃–polymer in the forms of films and fibrous mats are listed in Table I. A significant increase in the hydrophobicity of fibrous mats compared to the corresponding films is attributed to the voids between fibers that can trap air.³⁰ The contact angles of the films with perovskites are not significantly different from those of neat polymers, indicating that perovskites tend to be buried inside the polymers due to their high surface tension. For the neat polymer and perovskite–polymer

TABLE I. Contact angle values of the samples.

	SBS film	PMMA film	PS film	SBS fiber	PMMA fiber	PS fiber
Contact angle (deg)	81.29	67.98	85.2	104.35	117.35	134.66
	CsPbBr ₃ @SBS film	CsPbBr ₃ @PMMA film	CsPbBr ₃ @PS film	CsPbBr ₃ @SBS fiber	CsPbBr ₃ @PMMA fiber	CsPbBr ₃ @PS fiber
Contact angle (deg)	79.71	67.92	84.4	103.41	122.99	141.78

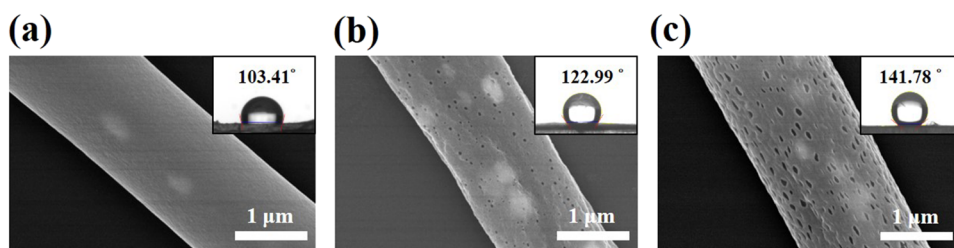


FIG. 4. The HRSEM images of (a) CsPbBr₃@SBS fiber, (b) CsPbBr₃@PMMA fiber, and (c) CsPbBr₃@PS fiber. The insets show the contact angles of the polymer fibers.

fibrous mats, the contact angle followed the order PS > PMMA > SBS. We used the high-resolution SEM (HRSEM) to observe the fibers, as illustrated in Figs. 4(a)–4(c), and found that the surfaces of the CsPbBr₃@PS and CsPbBr₃@PMMA fibers are porous, whereas the CsPbBr₃@SBS fibers are smooth. The porous structure may be responsible for the further enhancement of the hydrophobicity for PS and PMMA fibers.

B. Photoluminescence and stability

Figure S4 displays the photoluminescence (PL) spectra of the CsPbBr₃ QD-based fibers, and the data are summarized in Table II. The PL peaks of CsPbBr₃ in polymers were slightly redshifted from that of CsPbBr₃ QDs in nanofiber film, from 511 nm to 513, 515, and 516 nm for SBS, PMMA, and PS, respectively, as illustrated in Fig. S4. The redshift can be attributed to the aggregation of perovskite QDs, which facilitates nonradiative recombination.³¹ The redshift in the order of PS > PMMA > SBS and the photoluminescence quantum yield (PLQY) in reverse order (Table II) agree with the TEM images [Figs. 2(d)–2(f)], where CsPbBr₃@PS fibers show the severest aggregation.

Figure 5(a) displays the time-dependent PL intensity of the CsPbBr₃-polymer fibers under UV LED chip (405 nm) excitation for 6 h. The PL of the perovskites degraded under UV illumination due to the reaction with CO₂, O₂, and H₂O³² and the UV stability was found to be in the order of CsPbBr₃@PS > CsPbBr₃@PMMA > CsPbBr₃@SBS. To examine the water resistance, we immersed the samples in a water bath, and the PL intensity as a function of immersing time is shown in Fig. 5(b). The PL intensities dropped

to 0%, 50%, and 83% of the initial values for SBS, PMMA, and PS, respectively, after 3 months. Note that after 3 months, the PL peaks red-shifted possibly because of the faster degradation of the smaller QD populations that emit lights of shorter wavelengths. This is accompanied by a decrease in the full width at half maximum (FWHM) of the emissions as shown in Fig. S5. Both the above tests suggest that the rigid, hydrophobic PS can effectively avoid the diffusion of active gases and water into fibers to prevent the perovskites from degradation, while the SBS with soft polybutadiene segments provides less protection against those molecules. The superior UV and water stabilities of the CsPbBr₃@PS fibers are due to the fact that the higher hydrophobicity lowers the affinity between PS and the polar molecules, and the high rigidity at room temperature retard the motion of the molecules inside PS fibers.

Thermal stability is also a crucial index of perovskite-polymer composites, which was tested in the present study by monitoring the PL spectra under thermal circles. Figure 5(c) compares the PL intensity of the samples heated and then cooled between 20 and 120 °C. The PL intensity for all the samples decreased with increasing temperature and then increased upon cooling. The CsPbBr₃@PMMA fibers show the highest reversibility with nearly overlapped heating and cooling curves while the PL intensity of the CsPbBr₃@PS fibers is less than 40% of the initial value when cooling back to 20 °C after heating to 120 °C. Such a polymer-dependent thermal stability is correlated with the glass transition temperature T_g of the polymers. The T_g s of the fibers were determined using a dynamic mechanical analyzer (DMA) shown in Fig. S6. The T_g of CsPbBr₃@PMMA is 157 °C below which the PMMA chains are frozen and the

TABLE II. Preparation conditions and characteristics of the samples.

Sample	Polymer concentration (wt. %)	Diameter (μm) ^a	PL peak position (nm)	PL FWHM (nm) ^b	PLQY value (%)	CIE (X, Y)
CsPbBr ₃ QDs	NA	NA	511	20	70	(0.0623, 0.7155)
CsPbBr ₃ @SBS fiber	15	~1.5	513	21	29	(0.0736, 0.7116)
CsPbBr ₃ @PMMA fiber	15	~1.5	515	22	27	(0.0898, 0.7498)
CsPbBr ₃ @PS fiber	15	~1.5	516	23	23	(0.0873, 0.7373)
CsPbBr ₃ @SBS film	15	NA	515	22	26.7	(0.0777, 0.7398)
CsPbBr ₃ @PMMA film	15	NA	515	22	23.5	(0.0736, 0.7383)
CsPbBr ₃ @PS film	15	NA	515	21	22	(0.0791, 0.7381)

^aDiameter of the ES nanofiber.

^bThe line broadening at half the maximum intensity of the PL peak.

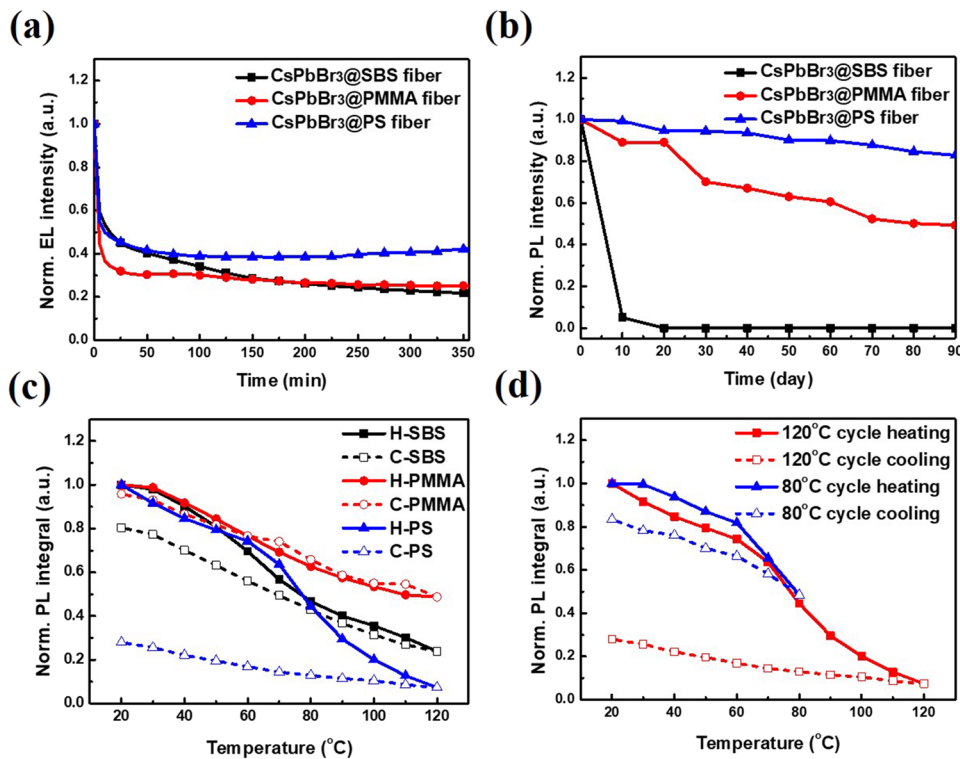


FIG. 5. (a) PL intensity of the samples measured under UV-chip LED (405 nm) excitation for 6 h. (b) PL intensity of the samples measured in water for 90 days. (c) Temperature-dependent PL intensity of the samples in the cycle from 20 to 120 °C [Heated (H) and cooled (C)]. (d) Temperature-dependent PL intensity of the CsPbBr₃@PS fiber measured in different temperature cycles (80 °C and 120 °C).

morphology inside the fibers is nearly fixed, which explains why the decay rate of the PL intensity is low upon heating and the reversibility is high below 120 °C. The T_g of CsPbBr₃@PS is 109 °C. In other words, the PS chains become mobile at 120 °C, which along with the low compatibility between PS and QDs causes the QDs to merge irreversibly, thus leading to the rapid decay of the PL intensity and the low reversibility. To confirm this argument, the CsPbBr₃@PS fibers were heated to 80 °C instead of 120 °C and the PL profiles are shown in Fig. 5(d). The reversibility can indeed be greatly improved when the thermal cycle was performed below T_g . CsPbBr₃@SBS fibers show two T_g s: -91 °C from polybutadiene segments and 112 °C from PS segments. The highly mobile polybutadiene segments that allow a faster diffusion of molecules are responsible for the low UV and water stability of CsPbBr₃@SBS fibers at room temperature as described above. However, the higher compatibility between polybutadiene and the QDs impart a better thermal stability and reversibility to CsPbBr₃@SBS fibers in comparison with CsPbBr₃@PS, even though SBS also bears PS segments.³³

Figure S7 shows the temperature-dependent PL data within the reversible temperature range from 78 K to 300 K, which were fitted by³⁴

$$I(T) = \frac{I_0}{1 + Ae^{-E_b/k_B T}}, \quad (1)$$

where I_0 is the intensity at 0 K, E_b is the exciton binding energy, k_B is Boltzmann constant, and higher E_b indicates a better dispersion of QDs in polymers. The E_b values for CsPbBr₃@SBS,

CsPbBr₃@PMMA, and CsPbBr₃@PS are 55, 46, and 39 meV, respectively. The low E_b for CsPbBr₃@PS fiber implies a poor dispersion of QDs in PS,^{35–37} consistent with the TEM images [Figs. 2(d)–2(f)].

Figure 6 shows the time-resolved PL of CsPbBr₃-based QDs and fibers. The curves were fitted with the following equation:

$$A(t) = A_1 \exp\left(\frac{-t}{\tau_1}\right) + A_2 \exp\left(\frac{-t}{\tau_2}\right), \quad (2)$$

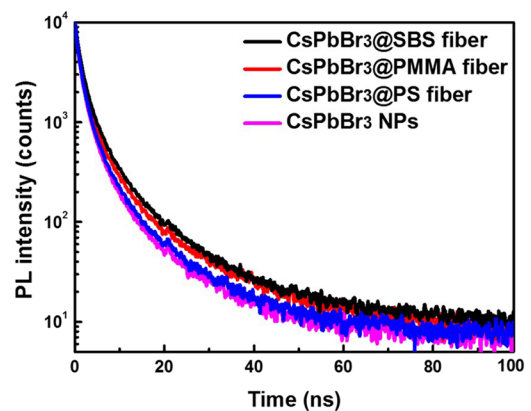


FIG. 6. Time-resolved PL spectra of CsPbBr₃@SBS fiber, CsPbBr₃@PMMA fiber, CsPbBr₃@PS fiber, and CsPbBr₃ NPs.

TABLE III. Time-resolved PL spectra of CsPbBr₃@SBS, CsPbBr₃@PMMA, CsPbBr₃@PS fiber, and CsPbBr₃ NPs.

	τ_1 (ns)	A ₁ (%)	τ_2 (ns)	A ₂ (%)	τ_{avg}
CsPbBr ₃ @SBS fiber	1.061 01	76	5.007 9	24	3.431 296
CsPbBr ₃ @PMMA fiber	0.947 23	78	4.709 87	22	3.169 109
CsPbBr ₃ @PS fiber	0.900 87	77	4.095 33	23	2.740 836
CsPbBr ₃ film	0.850 17	77	3.772 5	23	2.518 881

where τ_1 is the short-lived lifetime attributed to the intrinsic recombination, τ_2 is the long-lived lifetime from the surface-state recombination, and A₁ and A₂ are the fractions of the two different contributions. The fitting parameters are listed in Table III. τ_1 s were 0.8, 1.1, 0.9, and 0.9 ns and τ_2 s were 3.7, 5.0, 4.7, and 4.1 ns for CsPbBr₃ QDs, CsPbBr₃@SBS fiber, CsPbBr₃@PMMA fiber, and CsPbBr₃@PS fiber, respectively. τ_1 has been reported to reflect the trapping of excitons by crystal defects. The higher τ_1 for the CsPbBr₃-polymer fibers suggested that less nonradiative recombination occurred in the perovskite embedded in the fibers. τ_2 corresponds to the surface defects

of the perovskite crystals, and the perovskite-polymer fibers show greater probability of radiative recombination than the neat QDs, as implied by the higher τ_2 . As previously discussed, the polymers form a protection layer for the embedded perovskites such that the surface defects caused by CO₂, O₂, and H₂O in the ambient condition are reduced.

In sum, the above results suggest that the polymers can impart different characteristics to the perovskite-polymer fibers. CsPbBr₃@SBS fibers demonstrated the highest PLQY and the longest PL lifetime, which could be useful for applications in

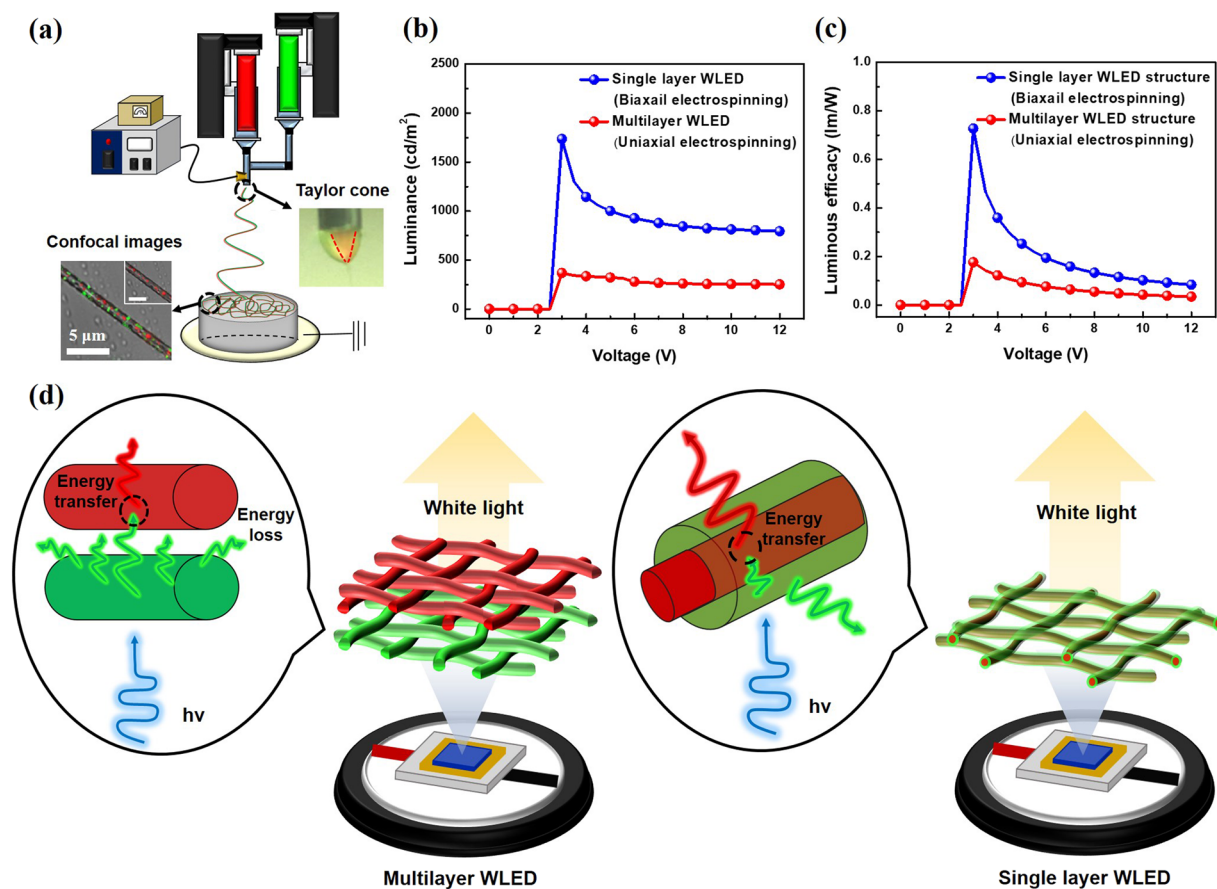


FIG. 7. (a) Illustration of the biaxial ES technique for fabricating core [CsPb(Br_{0.4}I_{0.6})₃@PS QDs]/shell (CsPbBr₃@PS QDs) light-emitting nanofibers. [(b) and (c)] Luminance and luminous efficacy of biaxial ES and uniaxial ES of the WLED. (d) Comparison of the luminance of multilayer and single layer WLED.

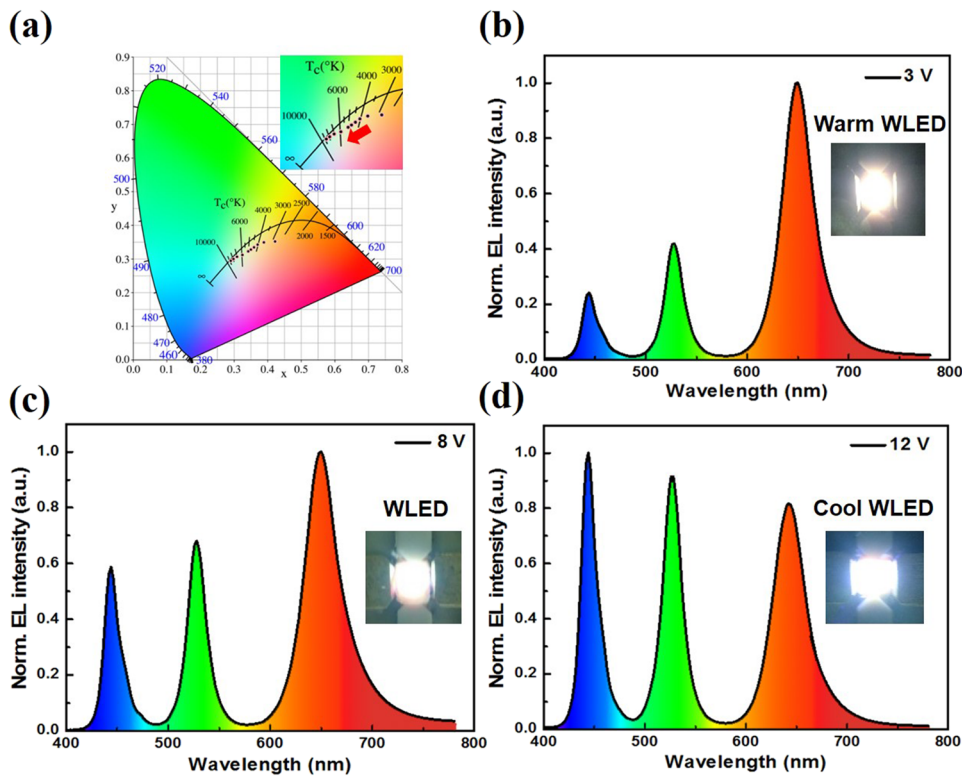


FIG. 8. (a) CIE color coordinates of white emission spectra. [(b)–(d)] Emission spectra of WLED, cool WLED, and warm WLED using core $[\text{CsPb}(\text{Br}_{0.4}\text{I}_{0.6})_3@PS$ QDs]/shell $(\text{CsPbBr}_3@PS$ QDs) fiber films under blue chip (450 nm) excitation. [(b)–(d)] Insets show the WLED, which was applied at voltages of 3, 8, and 12 V, corresponding to warm WLED, WLED, and cool WLED, respectively.

high-efficiency optoelectronic devices, and $\text{CsPbBr}_3@PMMA$ exhibited excellent thermal stability, which could be utilized in high-voltage LEDs. Although $\text{CsPbBr}_3@PS$ exhibited the shortest PL lifetime and the largest PL shift, it possessed the highest UV and water stability, which could provide constant fluorescent intensity under atmosphere.

C. White-light-emitting applications

We have demonstrated that the perovskite-polymer fibers are color-tunable and stable. We further developed white-light-emitting fibers prepared by the core/shell biaxial electrospinning in which the red and green perovskite materials served as the core and the shell, respectively. Figure 7(a) illustrates the setup and the process of the biaxial electrospinning. The Taylor cone with red $\text{CsPb}(\text{Br}_{0.4}\text{I}_{0.6})_3$ QDs @PS in the core and green CsPbBr_3 QDs @PS in the shell could be seen. The confocal image clearly shows the distinct red and green perovskites inside the fiber. The WLEDs were fabricated by using a single layer of core/shell fibrous mats on a commercial blue chip ($\lambda_{\text{max}} = 450$ nm), which were then compared with the devices with multilayers of single-colored green and red fibers, as illustrated in Fig. 7(d). The single layer of the core/shell fibers markedly enhanced the WLED performance and exhibited the luminance and efficiency of 400% higher than those of the multilayer structures, as shown in Figs. 7(b) and 7(c). The great improvement is attributed to the efficient energy transfer of photoluminescence between the perovskites in the core and shell inside the fibers [Fig. 7(d)]. Note that in Fig. 7(d), the multilayer means using

two kinds of fiber mats, red “ $\text{CsPb}(\text{Br}_{0.4}\text{I}_{0.6})_3$ QDs @PS” and “green CsPbBr_3 QDs @PS,” which were separated and collected on the LED chip. However, single layer means just using one kind of fiber mat, red $\text{CsPb}(\text{Br}_{0.4}\text{I}_{0.6})_3$ QDs @PS (core), and green CsPbBr_3 QDs @PS (shell), which were directly collected on the LED chip. Moreover, the fiber mat thickness of single-layered and multilayered WLED device is the same ($0.3 \text{ mm} \pm 0.05 \text{ mm}$) by controlling the collecting time of ES process.

The CIE color coordinates and CCT of WLEDs with a single layer of the core/shell fibers can be controlled by adjusting the voltages, which are shown in Fig. 8(a) and listed in Table S1. Furthermore, warm WLED, natural WLED, and cold WLED devices were successfully fabricated by adjusting the thicknesses of the fibrous mats under blue LED excitation [Figs. 8(b)–8(d)]. The insets in Figs. 8(b)–8(d) display the WLED devices with different CCTs. By controlling both the spacing between the LED chip and the fibrous mat and the porosity of the fibrous mats, the degradation of the temperature-sensitive perovskites can be reduced.³⁸ The packaging method developed in this work can enhance the device performance as well as improve the stability.

III. CONCLUSION

In summary, we adopted a simple electrospinning method by mixing cesium lead halide perovskite quantum dots and polymers to prepare stable luminescent fibers. The color can be tuned by changing the halide ratios in the perovskites, and the properties of the fibers are affected by the polymers. The higher compatibility

between QDs and SBS rubber leads to a better dispersion of the QDs in the fibers, the higher hydrophobicity of PS imparts higher UV and water stability to the perovskites, and the higher glass transition temperature of PMMA gives the superior thermal stability of the fibers. The optimized fibers with perovskite QDs in PS yielded a high PLQY of 23.3%, which surpassed the value of the thin-film counterpart. The PL intensity of the fibers retained 83% of initial intensity for 3 months when immersed in water. We further demonstrated a new biaxial electrospinning strategy to prepare core/shell fibers with red and green colors, respectively, which produce white light with high luminance and high efficiency when irradiated by a blue LED due to the efficient energy transfer of photoluminescence. These findings reveal the potential of the electrospinning techniques to fabricate stable and efficient luminescent perovskite fibers.

IV. EXPERIMENTAL SECTION

A. Materials

Oleylamine (primary amine, >98%), oleic acid (90%), cesium carbonate (99.995%), 1-octadecene (90%), lead(II) bromide, poly(styrene-butadiene-styrene) (SBS) ($M_w = 142\,000$), poly(methyl methacrylate) (PMMA) ($M_w = 350\,000$), polystyrene (PS) ($M_w = 192\,000$), and dichloromethane (99.5%) were purchased from Sigma Aldrich.

B. Preparation of CsPbX_3 ($X = \text{Cl, Br, and I}$)

For the preparation of the Cs-oleate precursor, CsCO_3 (0.2035 g) and oleic acid (0.625 ml) were dissolved in 1-octadecene (10 ml) and added to a 25-ml two-neck flask. The solution was heated under vacuum at 120°C for 1 h under stirring. After 1 h, the reaction flask was stored with N_2 , and the temperature was heated to 150°C . The Cs-oleate in 1-oleylamine solution was stored in N_2 until required for QD synthesis.

PbBr_2 (0.138 18 g) and 1-octadecyl (ODE) (10 ml) were added in a 25-ml two-neck flask under vacuum at 120°C for 1 h under stirring. After 1 h, the reaction flask was stored with N_2 , and oleylamine (1 ml) and oleic acid (1 ml) were added to stabilize the lead precursors and as-synthesized NCs. Subsequently, the flask was heated to 170°C , followed by rapid injection of 0.8 ml of Cs-oleate solution. The solution was then quenched in an ice bath after 5 s. After the temperature of the green colloidal solution was cooled to 25°C , it was centrifuged at 4000 rpm for 10 min to separate the upper solution and precipitates. Toluene (0.6 ml) was added to the solid precipitates to be stored under vacuum.

C. Preparation of the ES fibers and thin film

The polymer solution was fed into a plastic syringe and expelled using syringe pumps (KD Scientific Model 100, USA) at a feed rate of $0.8\text{--}1.0\text{ ml h}^{-1}$. The tip of the metallic needle was connected to a high-voltage power supply (Chargemaster CH30P SIMCO, USA) that was set at 12.4 kV during ES. When the syringe pumps started, the polymer solution was expelled from a metallic needle and formed a nanoscale fiber at high voltage. A piece of aluminum foil or quartz was placed 15 cm below the tip of the needle for 1 h to collect the ES

nanofibers. All experiments were performed at room temperature with a relative humidity of approximately 20%.

D. Preparation of the biaxial ES of core [$\text{CsPb}(\text{Br}_{0.4}\text{I}_{0.6})_3$ QDs]/shell (CsPbBr_3 QDs) nanofibers

Fabrication was similar to the uniaxial ES technique. Two syringes were used, and each syringe was connected to a separate needle; the diameters of the core and shell needles were 0.80 and 1.25 mm, respectively. The $\text{CsPb}(\text{Br}_{0.4}\text{I}_{0.6})_3$ @polymer solution was fed into the core syringe, and the CsPbBr_3 @polymer solution was fed into the shell syringe to form the two-fluid coaxial ES system, with feed rates of 0.6 and 0.8 ml h^{-1} , respectively. The tip of the metallic needle was connected to a high-voltage power supply that was set at 12.4 kV during ES. The same process condition was applied with a piece of aluminum foil or quartz placed 15 cm below the tip of the needle for 1 h to collect the ES nanofibers. All experiments were performed at room temperature with a relative humidity of approximately 20%. These processes were monitored by using a high-speed charge-coupled device camera (USA Xli 3M USB 2.0) to ensure that the core solution was wrapped by the shell solution.

E. Characterization

Characterization XRD patterns were recorded using Cu K α radiation ($\lambda = 1.5418\text{ \AA}$) on a D2 Bruker diffractometer operating at 40 kV and 20 mA. The morphologies of the polymer@ CsPbBr_3 nanofibers were characterized using a scanning electron microscope (Hitachi S-4700). Samples were coated with platinum prior to SEM characterization, and analysis was performed at an acceleration voltage of 15 kV. TEM images were obtained using a Hitachi H-7100 field emission electron microscope, operating at 75 kV. Fluorescence optical microscopy images were taken using a two-photon laser confocal microscope (Leica LCS SP5). PL spectra were measured by using a Fluorolog-3 spectrofluorometer (Horiba Jobin Yvon), and the CsPbBr_3 @polymer and $\text{CsPb}(\text{Br}_{0.4}\text{I}_{0.6})_3$ @polymer samples were excited at wavelengths of 350 and 460 nm, respectively. The water-resistant properties of the CsPbBr_3 @polymer fiber film were observed through contact angle measurement (Phoenix 300 Touch, GAT Scientific) of water droplets on the samples. The CIE color coordinates and CCT of the WLED spectra were measured by PR670 under ambient air conditions at 25°C . The calibration method was standard sunset light, which correlated with a color temperature of 2856 K to confirm instrument correctness. The TR-PL spectra were coupled to a spectrometer (Horiba iHR320) with a Hamamatsu C10910 streak camera and an M10913 slow single sweep unit. Temperature-dependent photoluminescence was measured with a pulsed diode-laser (PicoQuant LDH-D-C-375) at a repetition rate of 1 MHz (power density: $3.63\text{ }\mu\text{W cm}^{-2}$). The excitation wavelength was 375 nm. The samples were mounted in a liquid nitrogen cryostat (Janis ST-500-UC) in vacuum (10^{-6} Torr), and the sample was measured from 300 to 78 K.

SUPPLEMENTARY MATERIAL

See the [supplementary material](#) for the energy dispersive spectroscopy (EDS) mapping that was conducted for the CsPbBr_3 and $\text{CsPb}(\text{Br}_{0.4}\text{I}_{0.6})_3$ fiber films, HRTEM of the CsPbBr_3 fiber film was conducted, and confocal images of the CsPbBr_3 and $\text{CsPb}(\text{Br}_{0.4}\text{I}_{0.6})_3$

fiber films were recorded. The PL spectra of the samples, PL peak and FWHM of CsPbBr₃@PMMA fiber and CsPbBr₃@PS fiber, and DMA analysis of the CsPbBr₃-polymer fiber film were conducted. The low temperature-dependent PL was measured. Properties of WLED fabricated using core/shell biaxial perovskite@PS nanofibers with blue-chip LED ($\lambda_{\text{max}} = 450 \text{ nm}$) excitation under the operating current 10 mA were also discussed.

ACKNOWLEDGMENTS

This work was supported by the Ministry of Science and Technology, Taiwan (Contract Nos. MOST 106-2221-E-027-119-MY3, MOST 105-2221-E-027-134-MY3, and MOST 104-2113-M-027-007-MY3).

REFERENCES

- ¹A. Kojima, K. Teshima, Y. Shirai, and T. Miyasaka, *J. Am. Chem. Soc.* **131**(17), 6050 (2009).
- ²Y. Zhang, D. J. Hellebusch, N. D. Bronstein, C. Ko, D. F. Ogletree, M. Salmeron, and A. P. Alivisatos, *Nat. Commun.* **7**, 11924 (2016).
- ³G. H. Carey, A. L. Abdelhady, Z. Ning, S. M. Thon, O. M. Bakr, and E. H. Sargent, *Chem. Rev.* **115**(23), 12732 (2015).
- ⁴J. Burschka, N. Pellet, S.-J. Moon, R. Humphry-Baker, P. Gao, M. K. Nazeeruddin, and M. Grätzel, *Nat. Mater.* **4**(9), 316 (2013).
- ⁵J.-S. Lee, M. V. Kovalenko, J. Huang, D. S. Chung, and D. V. Talapin, *Nat. Nanotechnol.* **6**(6), 348 (2011).
- ⁶R. C. Somers, M. G. Bawendi, and D. G. Nocera, *Chem. Soc. Rev.* **36**(4), 579 (2007).
- ⁷V. L. Colvin, M. C. Schlamp, and A. P. Alivisatos, *Nature* **370**(6488), 354 (1994).
- ⁸B. Hailegnaw, S. Kirmayer, E. Edri, G. Hodes, and D. Cahen, *J. Phys. Chem. Lett.* **6**(9), 1543 (2015).
- ⁹M. Grätzel, *Nat. Mater.* **13**(9), 838 (2014).
- ¹⁰Y. Xin, H. Zhao, and J. Zhang, *ACS Appl. Mater. Interfaces* **10**(5), 4971 (2018).
- ¹¹Z. Li, L. Kong, S. Huang, and L. Li, *Angew. Chem.* **129**(28), 8246 (2017).
- ¹²A. Fakharuddin, F. Di Giacomo, A. L. Palma, F. Matteocci, I. Ahmed, S. Razza, A. D'Epifanio, S. Licoccia, J. Ismail, and A. Di Carlo, *ACS Nano* **9**(8), 8420 (2015).
- ¹³S. N. Raja, Y. Bekenstein, M. A. Koc, S. Fischer, D. Zhang, L.-Y. Lin, R. O. Ritchie, P. Yang, and A. P. Alivisatos, *ACS Appl. Mater. Interfaces* **8**(51), 35523 (2016).
- ¹⁴Q. Zhou, Z. Bai, W.-G. Lu, Y. Wang, B. Zou, and H. Zhong, *Adv. Mater.* **28**(41), 9163 (2016).
- ¹⁵Y. Wang, J. He, H. Chen, J. Chen, R. Zhu, P. Ma, A. Towers, Y. Lin, A. J. Gesquiere, and S.-T. Wu, *Adv. Mater.* **28**(48), 10710 (2016).
- ¹⁶M. Meyns, M. Perálvarez, A. Heuer-Jungemann, W. Hertog, M. Ibáñez, R. Nafria, A. Genç, J. Arbiol, M. V. Kovalenko, and J. Carreras, *ACS Appl. Mater. Interfaces* **8**(30), 19579 (2016).
- ¹⁷Y. Wei, X. Deng, Z. Xie, X. Cai, S. Liang, P. Ma, Z. Hou, Z. Cheng, and J. Lin, *Adv. Funct. Mater.* **27**(39), 1703535 (2017).
- ¹⁸D.-H. Jiang, P.-C. Tsai, C.-C. Kuo, F.-C. Jhuang, H.-C. Guo, S.-P. Chen, Y.-C. Liao, T. Satoh, and S.-H. Tung, *ACS Appl. Mater. Interfaces* **11**, 10118 (2019).
- ¹⁹P.-C. Tsai, J.-Y. Chen, E. Ercan, C.-C. Chueh, S.-H. Tung, and W.-C. Chen, *Small* **14**(22), 1704379 (2018).
- ²⁰Y.-W. Lin, C.-J. Lin, Y.-H. Chou, C.-L. Liu, H.-C. Chang, and W.-C. Chen, *J. Mater. Chem. C* **1**(34), 5336 (2013).
- ²¹P. Wang, L. Zhang, Y. Xia, L. Tong, X. Xu, and Y. Ying, *Nano Lett.* **12**(6), 3145 (2012).
- ²²J. Song, M. Chen, M. B. Olesen, C. Wang, R. Havelund, Q. Li, E. Xie, R. X. Yang, P. Bøggild, and C. Wang, *Nanoscale* **3**(12), 4966 (2011).
- ²³H. Jeong and J. K. Lee, *ACS Appl. Mater. Interfaces* **7**(51), 28459 (2015).
- ²⁴J.-Y. Chen, Y.-C. Chiu, C.-C. Shih, W.-C. Wu, and W.-C. Chen, *J. Mater. Chem. A* **3**(29), 15039 (2015).
- ²⁵C.-C. Kuo, C.-T. Wang, and W.-C. Chen, *Macromol. Mater. Eng.* **293**(12), 999 (2008).
- ²⁶C.-C. Lin, D.-H. Jiang, C.-C. Kuo, C.-J. Cho, Y.-H. Tsai, T. Satoh, and C. Su, *ACS Appl. Mater. Interfaces* **10**(3), 2210 (2018).
- ²⁷L. Protesescu, S. Yakunin, M. I. Bodnarchuk, F. Krieg, R. Caputo, C. H. Hendon, R. X. Yang, A. Walsh, and M. V. Kovalenko, *Nano Lett.* **15**(6), 3692 (2015).
- ²⁸C.-Y. Huang, C. Zou, C. Mao, K. L. Corp, Y.-C. Yao, Y.-J. Lee, C. W. Schlenker, A. K. Jen, and L.-Y. Lin, *ACS Photonics* **4**(9), 2281 (2017).
- ²⁹W. Chen, X. Xin, Z. Zang, X. Tang, C. Li, W. Hu, M. Zhou, and J. Du, *J. Solid State Chem.* **255**, 115 (2017).
- ³⁰M. Kang, R. Jung, H.-S. Kim, and H.-J. Jin, *Colloids Surf., A* **313**, 411 (2008).
- ³¹Y. Wang, X. Li, S. Sreejith, F. Cao, Z. Wang, M. C. Stuparu, H. Zeng, and H. Sun, *Adv. Mater.* **28**(48), 10637 (2016).
- ³²J. Li, L. Wang, X. Yuan, B. Bo, H. Li, J. Zhao, and X. Gao, *Mater. Res. Bull.* **102**, 86 (2018).
- ³³H. A. Shnawa, M. I. Khaleel, and F. J. Muhamed, *Open J. Polym. Chem.* **5**, 9–16 (2015).
- ³⁴K. Wu, A. Bera, C. Ma, Y. Du, Y. Yang, L. Li, and T. Wu, *Phys. Chem. Chem. Phys.* **16**(41), 22476 (2014).
- ³⁵D. Chen, S. Yuan, J. Chen, J. Zhong, and X. Xu, *J. Mater. Chem. C* **6**(47), 12864 (2018).
- ³⁶B. Ai, C. Liu, Z. Deng, J. Wang, J. Han, and X. Zhao, *Phys. Chem. Chem. Phys.* **19**(26), 17349 (2017).
- ³⁷X. Li, Y. Wu, S. Zhang, B. Cai, Y. Gu, J. Song, and H. Zeng, *Adv. Funct. Mater.* **26**(15), 2435 (2016).
- ³⁸S. E. Brinkley, N. Pfaff, K. A. Denault, Z. Zhang, H. Hintzen, R. Seshadri, S. Nakamura, and S. P. DenBaars, *Appl. Phys. Lett.* **99**(24), 241106 (2011).